Broadband plasmonic device concentrating the energy at the nanoscale: The crescent-shaped cylinder

Alexandre Aubry, Dang Yuan Lei, Stefan A. Maier, and J. B. Pendry
The Blackett Laboratory, Department of Physics, Imperial College London, London SW7 2AZ, United Kingdom
(Received 20 May 2010; published 16 September 2010)

A new strategy has been proposed recently to design broadband plasmonic nanostructures capable of a significant nanofocusing of light. Applying a singular conformal transformation to a thin slab of metal, a cylinder with a crescent-shaped cross section is obtained. In this study, the corresponding theory is derived analytically and different physical insights are provided to analyze the broadband light harvesting and nanofocusing properties of this device. The optical response of the crescent is deduced by solving the metal-slab problem. The nanostructure is shown to exhibit a continuous absorption cross section which redshifts for thin crescents due to a decrease of the surface plasmon velocity. The field enhancement induced by the nanostructure is also derived analytically. The nanofocusing performance is shown to result from a balance between dissipation losses and surface-plasmons velocity. This implies a strong dependence of the field enhancement on the frequency and the crescent geometry. Numerical simulations have also been performed to investigate the effect of radiative losses when the structure dimension becomes comparable to the wavelength. Radiative damping makes the absorption cross section saturate at the level of the physical cross section. The field enhancement decreases with the size of the device. The crescent structure is shown to be quite robust to radiation losses, which opens perspectives for applications such as single-molecule detection.

DOI: 10.1103/PhysRevB.82.125430 PACS number(s): 78.67.Bf, 73.20.Mf

I. INTRODUCTION

Since the pioneering work of Mie[1] and Ritchie,[2] there has been a vast amount of research efforts to investigate the electromagnetic properties of metal/dielectric interfaces (see, e.g., Refs. 3–6 and references therein). Such structures can support surface-plasmon polaritons (SPPs) which are light waves coupled to free-electron oscillations in the metal. This results in a strong confinement of light at the metal/dielectric interface. SPPs can show strong coupling to light and have wavelengths of only a few tens of nanometers, hence beating the classical diffraction limit. These unique properties have opened perspectives in nanophotonics. The subwavelength confinement of light near a flat dielectric/metal interface has been used for applications in evanescent surface sensors[7] or in integrated optical circuits.[8,9] Localized surface plasmons can also be excited in a metal particle. Stronger nanofocusing and local enhancement of the field can then be expected. In the literature, the strategy to obtain a maximum-field enhancement consists in combining a strong overall resonance of the structure with very small and sharp geometric features where hot spots will arise. Following this principle, several plasmonic structures have been investigated, such as triangles/squares with sharp corners,[10,11] nanoparticles separated by a narrow gap,[10,12–22] or crescent-shaped nanoparticles.[23–29] The significant field enhancement, that such structures may provide, has drawn considerable attention in surface-enhanced Raman spectroscopy[16,23,30,31] or enhanced fluorescent emission.[32] Until now, the theoretical description of the optical response of such structures has remained a challenge. Only numerical simulations have been performed and few qualitative arguments have been put forward to explain these numerical results. Another severe challenge for potential applications lies in the spectral bandwidth over which plasmonic particles can efficiently operate. Indeed, small devices tend to be efficient collectors at just a few resonant frequencies, contrary to an infinite structure that naturally shows a broadband spectrum.[5]

In a recent article,[33] a general strategy based on transformation optics has been proposed to design and study analytically plasmonic devices capable of (a) an efficient harvesting of light over a broadband spectrum both in the visible and the near infrared regimes; (b) a strong far-field to near-field conversion of energy, leading to a considerable field confinement and enhancement. This strategy is as follows: start with an infinite plasmonic system that naturally shows a broadband spectrum and then apply a mathematical transformation that converts the infinite structure into a finite one while preserving the spectrum. This approach has been illustrated by two examples: the crescent-shaped cylinder and the kissing cylinders.[33] Some results of the analytical calculations have been presented to show the power and the elegance of the conformal transformation tool. However, the demonstration has remained very general and no analytical proof has been provided.

In this paper, the corresponding theory is derived in detail for the crescent-shaped cylinder and different physical insights are provided to explain the broadband harvesting and nanofocusing properties of this device. The coupling of a dipole with SPPs supported by an infinite slab of metal is first investigated analytically [Fig. 1(a)]. Then, by applying a conformal transformation to this system, we deduce the behavior of SPPs in a cylinder with a crescent-shaped cross section and their coupling with the external field [Fig. 1(b)]. An analytical expression of the absorption cross section is derived. This plasmonic structure is shown to provide an efficient harvesting of light over a broadband spectrum that shifts toward red when the crescent gets thinner. This shift is explained by the decrease in SPPs' velocity for thin crescents. An expression of the electric field in the crescent ge-

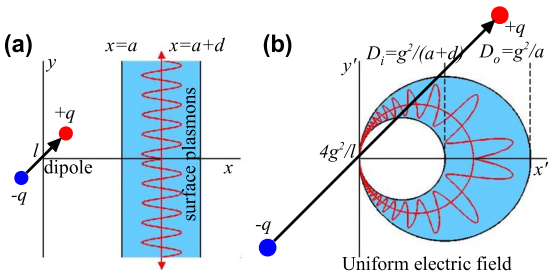

FIG. 1. (Color online) (a) A thin layer of metal supports SPPs that couple to a 2D dipole source, transporting its energy to infinity. (b) The transformed material is a cylinder with a cross section in the form of a crescent. The dipole source $\mathbf{\Delta}$ is transformed into a uniform electric field $\mathbf{E_0}$.

ometry is also derived analytically. The SPPs are shown to be excited in the fat part of the crescent and propagate along its claws toward the tip, where the group velocity vanishes and energy accumulates. The crescent is thus a strong far-field to near-field converter of energy: considerable field enhancement and confinement at the nanoscale is expected. The nanofocusing performance results from a balance between energy accumulation and dissipation losses. Hence, the field confinement and enhancement strongly depend on the frequency due to dissipation losses and on the crescent geometry due to the SPPs velocity. This analytical study relies on the near-field approximation which is valid as long as the crescent dimension is small compared to the wavelength. Consequently, numerical simulations have also been performed to investigate the effect of radiative losses for larger structure dimension. The crescent is shown to be quite robust relative to radiation damping, its absorption cross section remaining in the order of its physical cross section, for dimension up to 300 nm. Similarly, significant field enhancement is still obtained despite radiation losses.

II. ELECTROSTATIC THEORY

A. Conformal transformation

The conformal transformation leading to the crescent-shaped cylinder has already been presented in Ref. 33. We briefly recall the main points here. Our canonical system is a point dipole located near a thin layer of plasmonic material [Fig. 1(a)]. Now apply the following conformal transformation:

$$z' = \frac{g^2}{z^*}, \tag{1}$$

where $z=x+iy$ is the usual complex number notation and the superscript * stands for complex conjugate. The resulting structure is a cylinder with a crescent-shaped cross section [Fig. 1(b)]. The diameters of the inner and outer cylinders are, respectively,

$$D_i = \frac{g^2}{d+a}, \quad D_o = \frac{g^2}{a}. \tag{2}$$

We also define a key parameter,

$$\rho = D_i/D_o = \frac{a}{d+a}, \tag{3}$$

which is the ratio between the inner and outer diameters. The transformation of the source is also of particular importance. The original dipole $\mathbf{\Delta}$ is transformed into a uniform electric field,[33]

$$\mathbf{E}_0' = \frac{1}{2\pi\epsilon_0}\frac{\mathbf{\Delta}}{g^2}. \tag{4}$$

We shall assume that the dimensions of the crescent is sufficiently small that the surface-plasmon modes are well described in the near-field approximation. In this case, the uniform electric field can be taken as due to an incident plane wave. Moreover, the dielectric properties of the nanostructure are the same as those of the slab from which it is derived. Also preserved under the transformation is the electrostatic potential

$$\phi(x,y) = \phi'(x',y'). \tag{5}$$

The mathematics of the conformal transformation closely links the physics at work in each of the very different geometries. We will first solve the relatively tractable slab problem and then deduce the solution for the crescent geometry.

B. Coupling of a dipole to a metallic sheet

The coupling of a dipole to a metallic sheet is first addressed. The near-field approximation is made, hence we assume that the Laplace's equation is obeyed. The dipole $\mathbf{\Delta}$ consists of two line charges. We wish to calculate the potential ϕ induced on the dielectric sheet by expanding the incident field ϕ_o of the dipole as a Fourier series in y

$$\phi_o(\mathbf{r}) = -\frac{1}{2\pi\epsilon_0}\frac{\mathbf{\Delta}\cdot\mathbf{r}}{r^2} = \frac{1}{2\pi}\int dk\,\phi_o(k)e^{iky}. \tag{6}$$

$\phi_o(k)$ can be found by making a Fourier transform in a transverse plane at an arbitrary position x

$$\phi_o(k) = \int \phi_o(x,y)e^{-iky}dy = a(k)e^{-|k||x|}, \tag{7}$$

with

$$a(k) = \frac{-\operatorname{sgn}(x)\Delta_x + i\operatorname{sgn}(k)\Delta_y}{2\epsilon_0}. \tag{8}$$

Next we calculate the field $\phi(k)$ induced by the metal plate located between $a<x<a+d$. As illustrated by Fig. 2, this field can be expressed as follows:

$$\phi(k) = \begin{cases} b(k)e^{|k|x}, & x < a \\ c(k)e^{-|k|x} + d(k)e^{|k|x}, & a < x < a+d \\ e(k)e^{-|k|x}, & x > a+d. \end{cases} \tag{9}$$

The four unknowns $b(k)$, $c(k)$, $d(k)$, and $e(k)$ are then determined by the boundary conditions at the dielectric slab interfaces. Two are derived from the parallel component of the electric field being conserved at a boundary,

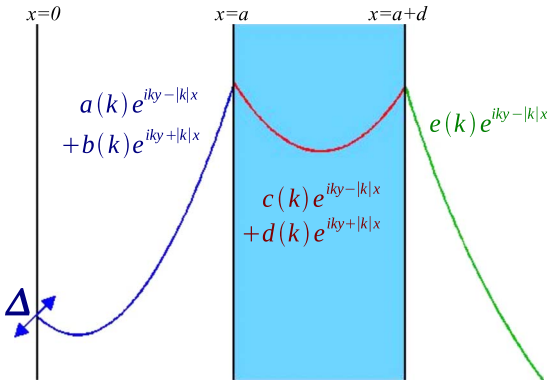

FIG. 2. (Color online) Sketch of the electrostatic potential induced in a metallic slab by a dipole $\mathbf{\Delta}$ at $x=0$ for $\epsilon<-1$.

$$a(k)e^{-|k|a} + b(k)e^{|k|a} = c(k)e^{-|k|a} + d(k)e^{|k|a},$$

$$c(k)e^{-|k|(a+d)} + d(k)e^{|k|(a+d)} = e(k)e^{-|k|(a+d)}$$

and two from conservation of the normal component of the displacement field,

$$a(k)e^{-|k|a} - b(k)e^{|k|a} = \epsilon[c(k)e^{-|k|a} - d(k)e^{|k|a}],$$

$$\epsilon[c(k)e^{-|k|(a+d)} - d(k)e^{|k|(a+d)}] = e(k)e^{-|k|(a+d)}.$$

Solving these four equations provides the following results:

$$b(k) = \frac{\epsilon-1}{\epsilon+1}\frac{e^{-2|k|a}(1-e^{2|k|d})}{e^{2|k|d}-e^{2\alpha}}a(k), \tag{10}$$

$$c(k) = \frac{2}{\epsilon+1}\frac{e^{2|k|d}}{e^{2|k|d}-e^{2\alpha}}a(k), \tag{11}$$

$$d(k) = \frac{2(\epsilon-1)}{(\epsilon+1)^2}\frac{e^{-2|k|a}}{e^{2|k|d}-e^{2\alpha}}a(k), \tag{12}$$

$$e(k) = \frac{4\epsilon}{(\epsilon+1)^2}\frac{e^{2|k|d}}{e^{2|k|d}-e^{2\alpha}}a(k), \tag{13}$$

where we have introduced,

$$e^{2\alpha} = \left(\frac{\epsilon-1}{\epsilon+1}\right)^2. \tag{14}$$

The dispersion of the excitations can be found from the condition that $b(k)$ diverges,

$$|k|d = \alpha = \begin{cases} \ln\left(\dfrac{\epsilon-1}{\epsilon+1}\right), & \text{if } \mathrm{Re}[\epsilon] < -1 \\ \ln\left(\dfrac{1-\epsilon}{\epsilon+1}\right), & \text{if } -1 < \mathrm{Re}[\epsilon] < 1. \end{cases} \tag{15}$$

This is the classical dispersion relation for SPPs in an insulator-metal-insulator structure upon the near-field approximation.

Now that the induced potential is known in the k space, it can be deduced in the real space via an inverse Fourier transform,

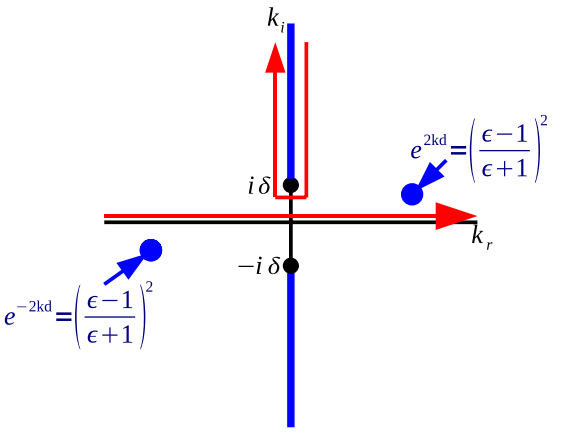

FIG. 3. (Color online) Analytic structure of the integrand of Eq. (17). There are two cuts running from $-i\delta$ and $+i\delta$ along the imaginary axis. There are also two poles if $\epsilon<0$ (disks). If $\epsilon>0$, these poles vanish in the cuts and give no contribution. Note that if $\epsilon<-1$, the poles are correctly placed but they swap to opposite sides of the real axis if $\epsilon>-1$.

$$\phi(x,y) = \frac{1}{2\pi}\begin{cases} \displaystyle\int b(k)e^{iky+|k|x}dk, & x<a \\ \displaystyle\int [c(k)e^{-|k|x} + d(k)e^{|k|x}]e^{iky}dk, & a<x<d+a \\ \displaystyle\int e(k)e^{iky-|k|x}dk, & x>d+a. \end{cases} \tag{16}$$

Let us tackle with the field induced at the dipole, i.e., for $x<a$. By injecting the expressions of $a(k)$ [Eq. (8)] and $b(k)$ [Eq. (10)], we obtain

$$-\phi(x<a) = \frac{1}{4\pi\epsilon_0}\frac{\epsilon-1}{\epsilon+1} \times \int [\Delta_x - i\,\mathrm{sgn}(k)\Delta_y]\frac{e^{-2|k|a}(1-e^{2|k|d})}{e^{2|k|d}-e^{2\alpha}} \times e^{iky+|k|x}dk. \tag{17}$$

To perform this integration, we write

$$|k| = \lim_{\delta\to 0}(k^2+\delta^2)^{1/2}.$$

The analytic structure of Eq. (17) is shown in Fig. 3. We shall make the approximation that the integral is dominated by either of the poles close to the real axis which correspond to surface-plasmon modes carrying away energy to infinity. The cuts correspond to localized virtual excitations which, if ϵ is real, dissipate no energy. Therefore in the limit of real ϵ our expression for dissipation will be exact, but otherwise only approximate. Therefore, from now, we will only consider the frequency band below the surface-plasmon frequency, $\omega<\omega_{sp}$, for which $\epsilon<-1$. Actually, beyond ω_{sp}, the imaginary part ϵ_I of the metal permittivity becomes compa-

rable to its real part ϵ_R and the contribution from the cuts shown in Fig. 3 is no longer negligible.

The calculation of the integral in Eq. (17) leads to

$$-\phi(x<a)=\frac{1}{d\epsilon_0}\frac{\epsilon}{\epsilon^2-1}[i\Delta_x+\mathrm{sgn}(y)\Delta_y]e^{\alpha(x-2a)/d}e^{i\alpha|y|/d}. \tag{18}$$

The same technique of integration can be used to compute the field ϕ for $x>a$. It yields

$$-\phi(a<x<a+d)=\frac{1}{2d\epsilon_0}[i\Delta_x+\mathrm{sgn}(y)\Delta_y]\left[\frac{e^{-\alpha x/d}}{\epsilon+1}+\frac{e^{\alpha(x-2a)/d}}{\epsilon-1}\right]e^{i\alpha|y|/d}, \tag{19}$$

$$-\phi(x>a+d)=\frac{1}{d\epsilon_0}\frac{\epsilon}{(\epsilon+1)^2}[i\Delta_x+\mathrm{sgn}(y)\Delta_y]e^{-\alpha x/d}e^{i\alpha|y|/d}. \tag{20}$$

C. Electric field induced at the dipole and dipolar moment of the crescent

From the expression of the induced potential ϕ for $x<a$ [Eq. (18)], we can deduce the electric field at the dipole

$$\mathbf{E}(z=0)=-\nabla\phi(z=0)=\frac{i\alpha}{d^2\epsilon_0}\frac{\epsilon}{\epsilon^2-1}e^{-2\alpha a/d}\mathbf{\Delta}. \tag{21}$$

This electric field induced at the dipole is of particular interest, since it is directly related to the net dipole moment $\mathbf{p}$ of the crescent in the transformed geometry. Indeed, similarly to the relation linking the emitting dipole $\mathbf{\Delta}$ to a uniform electric field $\mathbf{E_0'}$ in the crescent geometry [Eq. (4)], the dipole moment $\mathbf{p}$ can be deduced from $\mathbf{E}(z=0)$,

$$\mathbf{p}=2\pi\epsilon_0 g^2\mathbf{E}(z=0). \tag{22}$$

Injecting the expression of $\mathbf{E}(z=0)$ [Eq. (21)] into the last equation, replacing $\mathbf{\Delta}$ by its expression [Eq. (4)] and using the fact that $g^2/d=\rho D_o/(1-\rho)$ and $a/d=\rho/(1-\rho)$ [Eqs. (2) and (3)], the induced dipole moment can be expressed as the product of a polarizability with the incident electric field $\mathbf{E_0'}$ in the transformed frame,

$$\mathbf{p}=\underbrace{i4\pi^2\epsilon_0\left(\frac{\rho}{1-\rho}\right)^2 D_o^2\alpha\frac{\epsilon}{\epsilon^2-1}e^{-2\alpha\rho/(1-\rho)}}_{\text{polarizability }\gamma}\mathbf{E_0'}. \tag{23}$$

D. Absorption cross section

Dipoles and fields exchange roles in the two frames, but the product is unchanged. Therefore, energy dissipation is the same in each geometry. In the slab frame, the dipole energy pumped into the SPPs [Fig. 1(a)] can be calculated from the electric field due to the excited modes evaluated at the dipole[34,35]

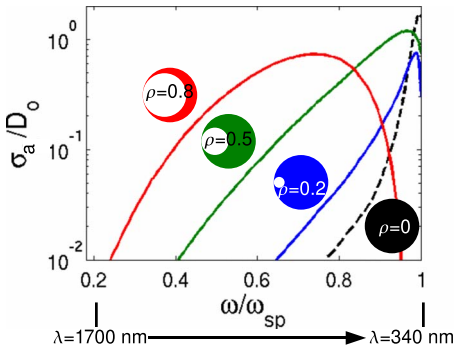

FIG. 4. (Color online) Absorption cross section as a fraction of the physical cross section as a function of frequency for different shapes of crescents (ρ=0.2 in blue, ρ=0.5 in green, and ρ=0.8 in red) with D_o=20 nm. The metal is assumed to be silver with a surface plasma frequency ω_{sp}=3.67 eV and permittivity taken from Johnson and Christy (Ref. 37). The absorption spectrum of one individual cylinder (Ref. 38) is also shown for comparison (dashed black line).

$$P=-\frac{\omega}{2}\mathrm{Im}\{\Delta^*\cdot\mathbf{E}(z=0)\}. \tag{24}$$

This dipole power dissipated maps directly onto the power absorbed by the crescent from the uniform electric field $\mathbf{E_0'}$ that we shall take as due to an incident plane wave in the transformed frame,[36]

$$P=-\frac{\omega}{2}\mathrm{Im}\{\mathbf{E_0'}^*\cdot\mathbf{p}\}. \tag{25}$$

If we inject the expression of $\mathbf{p}$ [Eq. (23)] into the last equation and renormalize it by the incoming flux $P_{in}=\epsilon_0 c_0|\mathbf{E_0'}|^2/2$, the absorption cross section $\sigma_a=P/P_{in}$ of the crescent can be deduced

$$\sigma_a=4\pi^2k_0^2\left(\frac{\rho}{1-\rho}\right)^2 D_o^2\,\mathrm{Re}\left\{\ln\left(\frac{\epsilon-1}{\epsilon+1}\right)\frac{\epsilon}{1-\epsilon^2}\left(\frac{\epsilon-1}{\epsilon+1}\right)^{-2\rho/1-\rho}\right\},$$
$$\text{if } \mathrm{Re}[\epsilon]<-1, \tag{26}$$

where we have replaced α by its expression as a function of the permittivity ϵ [Eq. (15)]. $k_0=\omega/c_0$ is the wave number in vacuum. Note that, rigorously, this expression corresponds to the extinction cross section of the crescent. However, as radiation losses are neglected under the quasistatic approximation, this quantity is here strictly equivalent to the absorption cross section. Note also that all orientations of the incident electric field are equally effective at excitation. The absorption cross section scales as the square of the physical size D_o of the crescent, which is typical of a two-dimensional configuration.

Figure 4 displays the absorption cross section σ_a as a fraction of the physical cross section for D_o=20 nm. For this figure as well as in the following of the study, the metal is assumed to be silver with a surface plasma frequency ω_{sp}=3.67 eV and permittivity taken from Johnson and Christy.[37] As already pointed out by Aubry *et al.*,[33] the crescent exhibits a broadband spectrum that shifts toward red

when the crescent gets thinner. Physically, this redshift can be explained by means of the velocity of SPPs along the crescent. As we will see in Sec. II E, the SPPs' velocity decreases when the crescent gets thinner and the dissipation losses tend to increase when we approach the surface-plasmon frequency. Hence, in a thin crescent, SPPs cannot propagate in the nanostructure when $\omega \to \omega_{sp}$. This explains the weak coupling of thin crescents with an external field at the vicinity of the surface-plasmon frequency.

Note that the crescent is a powerful light-harvesting device over a broadband spectrum both in the near infrared and visible regimes ($\lambda \sim 340 \to 1700$ nm, see Fig. 4). The broadband feature is highlighted by the comparison with the single cylinder case in Fig. 4. The absorption cross section of the crescent is on the order of the physical cross section even for such a small particle size ($D_o = 20$ nm). For constant ratio ρ, σ_a / D_o scales linearly with D_o. Thus cross sections higher than the physical size could be obtained for larger diameter crescents but in this case our near-field analytic theory may not be valid.[33]

E. Electric field in the transformed geometry

A cylinder with a crescent-shaped cross section is a nanostructure capable of an efficient harvesting of light over the visible and near-infrared spectra. As we will see now, this is also a strong far-field to near-field converter of energy, providing a considerable confinement and amplification of the electric field in the vicinity of its physical singularity.

Under the conformal transformation, the potential is preserved [Eq. (5)]. The electric field $\mathbf{E}'(x',y')$ in the crescent can then be easily deduced from the potential,

$$E'_{u'} = -\frac{\partial \phi}{\partial x}\frac{\partial x}{\partial u'} - \frac{\partial \phi}{\partial y}\frac{\partial y}{\partial u'} \tag{27}$$

with $u' = x', y'$. Using the expression of the potential ϕ given in Eqs. (18)–(20), the electric field $\mathbf{E}'$ can be expressed as a function of $\mathbf{E}'_0$ [Eq. (4)], D_o [Eq. (2)], and ρ [Eq. (3)]. It yields for $\epsilon < -1$,

(1) For $|z' - D_o/2| > D_o/2$ (outside the crescent):

$$E'_{x'} = 2\pi \ln\left(\frac{\epsilon-1}{\epsilon+1}\right)\frac{\epsilon}{1-\epsilon^2}\left(\frac{\epsilon-1}{\epsilon+1}\right)^{-2\rho/1-\rho}\frac{\rho^2}{(1-\rho)^2}\frac{D_o^2}{(x'-i|y'|)^2} \times [iE_{0x'} + \mathrm{sgn}(y')E_{0y'}]\exp\left(\frac{\alpha\rho}{1-\rho}\frac{D_o}{(x'-i|y'|)}\right), \tag{28}$$

$$E'_{y'} = 2\pi \ln\left(\frac{\epsilon-1}{\epsilon+1}\right)\frac{\epsilon}{1-\epsilon^2}\left(\frac{\epsilon-1}{\epsilon+1}\right)^{-2\rho/1-\rho}\frac{\rho^2}{(1-\rho)^2}\frac{D_o^2}{(x'-i|y'|)^2} \times [\mathrm{sgn}(y')E_{0x'} - iE_{0y'}]\exp\left(\frac{\alpha\rho}{1-\rho}\frac{D_o}{(x'-i|y'|)}\right). \tag{29}$$

(2) For $|z' - D_o/2| < D_o/2$ and $|z' - D_i/2| > D_i/2$ (in the metal):

$$E'_{x'} = \pi\frac{\rho^2}{(1-\rho)^2}\ln\left(\frac{\epsilon-1}{\epsilon+1}\right)[iE_{0x'} + \mathrm{sgn}(y')E_{0y'}] \times \left[\frac{1}{\epsilon+1}\frac{D_o^2}{(x'+i|y'|)^2}\exp\left(-\frac{\alpha\rho}{1-\rho}\frac{D_o}{(x'+i|y'|)}\right) + \frac{1}{1-\epsilon}\left(\frac{\epsilon-1}{\epsilon+1}\right)^{-2\rho/1-\rho}\frac{D_o^2}{(x'-i|y'|)^2} \times \exp\left(\frac{\alpha\rho}{1-\rho}\frac{D_o}{(x'-i|y'|)}\right)\right], \tag{30}$$

$$E'_{y'} = \pi\frac{\rho^2}{(1-\rho)^2}\ln\left(\frac{\epsilon-1}{\epsilon+1}\right)[\mathrm{sgn}(y')E_{0x'} - iE_{0y'}] \times \left[-\frac{1}{\epsilon+1}\frac{D_o^2}{(x'+i|y'|)^2}\exp\left(-\frac{\alpha\rho}{1-\rho}\frac{D_o}{(x'+i|y'|)}\right) + \frac{1}{1-\epsilon}\left(\frac{\epsilon-1}{\epsilon+1}\right)^{-2\rho/1-\rho}\frac{D_o^2}{(x'-i|y'|)^2} \times \exp\left(\frac{\alpha\rho}{1-\rho}\frac{D_o}{(x'-i|y'|)}\right)\right]. \tag{31}$$

(3) For $|z' - D_i/2| < D_i/2$ (inside the crescent):

$$E'_{x'} = 2\pi\frac{\epsilon}{(\epsilon+1)^2}\frac{\rho^2}{(1-\rho)^2}\ln\left(\frac{\epsilon-1}{\epsilon+1}\right)\frac{D_o^2}{(x'+i|y'|)^2} \times [iE_{0x'} + \mathrm{sgn}(y')E_{0y'}]\exp\left(-\frac{\alpha\rho}{1-\rho}\frac{D_o}{(x'+i|y'|)}\right). \tag{32}$$

$$E'_{y'} = -2\pi\frac{\epsilon}{(\epsilon+1)^2}\ln\left(\frac{\epsilon-1}{\epsilon+1}\right)\frac{\rho^2}{(1-\rho)^2}\frac{D_o^2}{(x'+i|y'|)^2} \times [\mathrm{sgn}(y')E_{0x'} - iE_{0y'}]\exp\left(-\frac{\alpha\rho}{1-\rho}\frac{D_o}{(x'+i|y'|)}\right). \tag{33}$$

In the near-field approximation, which holds when the dimensions of the crescent are less than the wavelength, the enhancement of electric field is independent of the size of the system. Figure 5 shows the result of our analytical calculation of the field distribution in the crescent for different frequencies and ratios ρ. The metal is still assumed to be silver with permittivity taken from Johnson and Christy.[37] These field distributions can be easily interpreted with conformal transformation as already discussed in Ref. 33. Here, we briefly recall the main points. In the slab frame, the surface-plasmon modes transport the energy of the dipole out to infinity (see Fig. 1). In the transformed frame, the same modes are excited in the fat part of the crescent and then propagate around the claws in an adiabatic fashion. As SPPs propagate toward the structure singularity, their wavelength shortens and velocity decreases in proportion, similarly to what happens in sharp metallic tips or grooves.[39–41] This brief qualitative account is confirmed by our analytical calculation. Considering Eqs. (28) and (29) at the surface of the crescent,

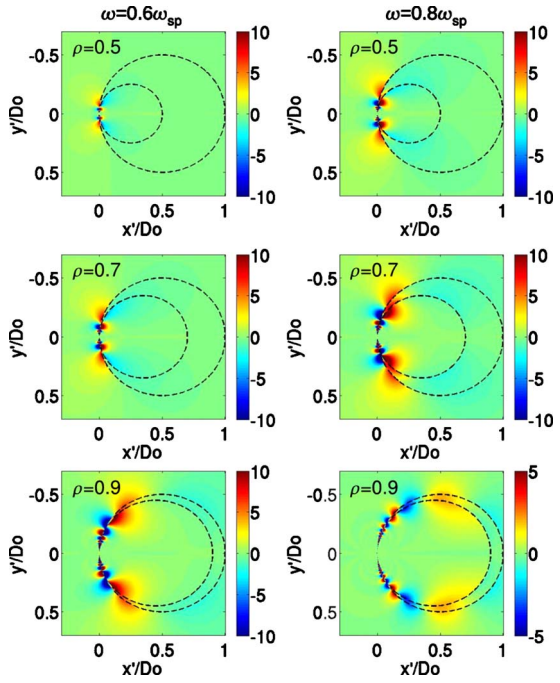

FIG. 5. (Color online) Amplitude of the real part of $E'_{x'}$ normalized by the incoming field E'_0 (polarized along x') at different frequencies ($\omega=0.6\omega_{sp}$ and $0.8\omega_{sp}$) and shapes of crescent ($\rho=0.5$, 0.7, and 0.9). The color scale is restricted to [−10 10] but note that the field magnitude is by far larger around the singularity of the structures.

one can show that the phase ϕ_{sp} of SPPs along the crescent surface varies as

$$\phi_{sp}(\theta) = \alpha \frac{\rho}{1-\rho} \tan(\theta/2), \tag{34}$$

where the angle θ is defined in the inset of Fig. 6(a). This expression confirms that the SPPs wavelength and velocity, proportional to $(d\phi_{sp}/d\theta)^{-1}$, vanish at the structure singularity ($\theta=\pi$). The dependence in α provides the dispersion relation of SPPs which is strictly equivalent to the one derived in the slab geometry [Eq. (15)]. At last, the term $\rho/(1-\rho)$ implies a decreasing of SPPs wavelength and velocity when the crescent gets thinner ($\rho \to 1$). As pointed out previously in Sec. II D, this fact explains the shift toward red of the absorption spectrum for finer crescents. As we will see in Sec. II F, the crescent shape has also a strong influence on the nanofocusing properties of the device.

In an ideal lossless metal, the cancellation of the SPPs velocity would lead to an accumulation of energy at the structure singularity. In practice finite loss resolves the situation leading to a balance between energy accumulation and dissipation.[33] Figure 5 shows that the field confinement around the structure singularity strongly depends on the frequency ω and the crescent geometry. The physical mechanisms governing the nanofocusing performance of the crescent are discussed in the following section.

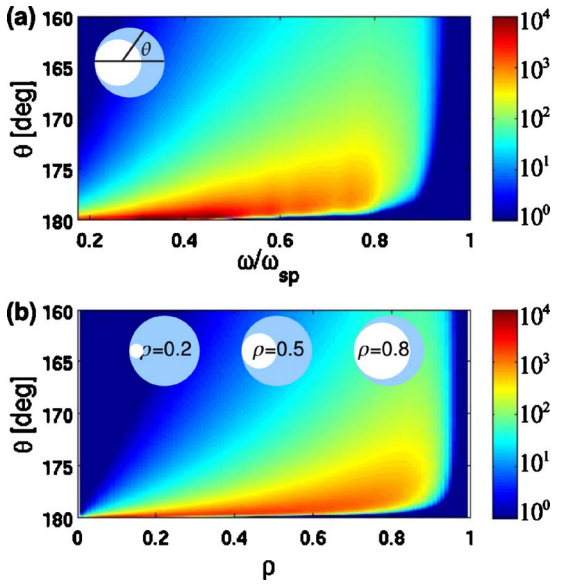

FIG. 6. (Color online) (a) Field enhancement, $|E'|/E'_0$, along the crescent surface as a function of the angle θ and frequency for $\rho=0.8$. (b) Field enhancement, $|E'|/E'_0$, along the crescent surface as a function of the angle θ and ρ for $\omega=0.75\omega_{sp}$. For both panels, the color bar is in log scale.

F. Field enhancement at the surface of the crescent

The evaluation of Eqs. (28) and (29) at the surface of the crescent provides an expression for the field enhancement $|E'|/E'_0 = \sqrt{|E'_{x'}|^2 + |E'_{y'}|^2}/E'_0$ as a function of the angle θ, defined in Fig. 6(a),

$$\left|\frac{E'}{E'_0}\right| = 2\pi\sqrt{2}\frac{\rho^2}{(1-\rho)^2}\left|\ln\left(\frac{\epsilon-1}{\epsilon+1}\right)\frac{\epsilon}{1-\epsilon^2}\left(\frac{\epsilon-1}{\epsilon+1}\right)^{-\rho/1-\rho}\right| \times \frac{\exp\left(-\frac{\rho}{1-\rho}\mathrm{Im}\{\alpha\}|\tan(\theta/2)|\right)}{\cos^2(\theta/2)}. \tag{35}$$

The effect of dissipation losses appears in the exponential term of the last equation: they truncate the growth of the field when surface-plasmons approach the structure singularity ($\theta=\pi$). From Eq. (35), the angle θ_{max} at which the maximum field enhancement occurs can be easily deduced,

$$\theta_{max} = \pi - \mathrm{a}\sin\left(\frac{\rho}{1-\rho}\mathrm{Im}\{\alpha\}\right). \tag{36}$$

Using the fact that $\mathrm{Im}\{\alpha\} = \mathrm{a}\tan[2\epsilon_I/(|\epsilon|^2-1)]$, θ_{max} can be explicitly expressed as a function of the permittivity imaginary part ϵ_I,

$$\theta_{max} \simeq \pi - \frac{2\rho}{1-\rho}\frac{\epsilon_I}{|\epsilon|^2-1}, \quad \text{if } \epsilon_I \ll |\epsilon|^2 - 1. \tag{37}$$

This expression of θ_{max} shows that an increase in the dissipation losses makes the maximum field enhancement shift to smaller angles, resulting in a worse confinement of the field around the structure singularity. θ_{max} also depends on the crescent geometry through the term $\rho/(1-\rho)$: when the crescents gets thinner ($\rho \to 1$), the field tends to spread spatially

along the crescent surface. This is explained by the decrease in the SPPs wavelength and velocity for thinner crescents [Eq. (34)]: the SPPs are then absorbed before getting close to the crescent tips in this case.

By injecting the expression of θ_{max} [Eq. (37)] into Eq. (35), one can deduce the maximum field enhancement, $|E'_{max}/E'_0|$, that can be expected at the surface of the crescent

$$\left|\frac{E'_{max}}{E'_0}\right| \simeq \frac{2\pi\sqrt{2}}{e^2}\left|\ln\left(\frac{\epsilon-1}{\epsilon+1}\right)\frac{\epsilon}{1-\epsilon^2}\left(\frac{\epsilon-1}{\epsilon+1}\right)^{-\rho/1-\rho}\right| \times\frac{(|\epsilon|^2-1)^2}{\epsilon_I^2}, \quad \text{if } \epsilon_I \ll |\epsilon|^2-1. \tag{38}$$

This expression shows that the dissipation losses reduces the growth of the field as the inverse square of the permittivity imaginary part ϵ_I.

Figure 6(a) displays the field enhancement [Eq. (35)] along the crescent surface as a function of frequency, calculated using the Johnson and Christy data.[37] At low frequencies, the field is strongly confined in the vicinity of the touching point and a spectacular field enhancement larger than 10^4 is predicted. This enhancement then decreases with frequency due to the increase in dissipation losses in silver when we approach the surface-plasmon frequency. Figure 6(b) displays the field enhancement along the crescent surface as a function of the ratio ρ. As explained previously, the lower velocity of SPPs when the crescent gets thinner implies a spatial spreading of the electric field. The magnitude of the enhancement is thus determined by how far around the nanostructure the wave field can propagate before being absorbed.

Note that the field enhancement displayed by Fig. 6 may be unrealistic in practice. There are indeed two limits to our electrostatic model. (i) A microscale limit: when the size of the device becomes comparable with the wavelength, radiation losses are no longer negligible and will reduce the field enhancement induced by the nanostructure. This point will be discussed in Sec. III. (ii) A nanoscale limit: at small length scales, continuum electrodynamics is no longer valid and nonlocal effects will play a role especially at the tips of the crescent, where the imaginary part of the dielectric function will increase.[42] This increase in ϵ_I will truncate the growth of the field along the crescent surface and reduce the field enhancement compared to our theoretical prediction [Eq. (38)].

III. RADIATION LOSSES

We now investigate the effect of radiation losses on the harvesting and nanofocusing performances of the crescent. As already shown in Ref. 33, radiation losses make the absorption cross section falls compared to our theoretical predictions when the structure dimension becomes comparable to the wavelength. Nevertheless, we will show, by means of numerical simulations, that the crescent structure is quite robust to radiation losses. This fact is important in perspective of future experiments.

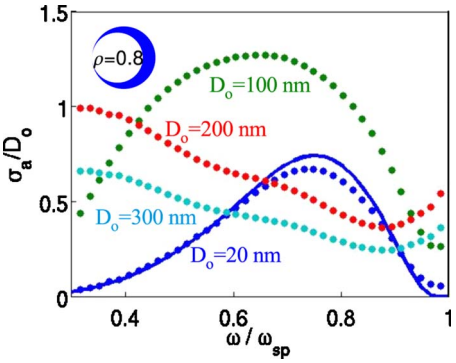

FIG. 7. (Color online) Absorption cross section normalized by the physical cross section as a function of frequency for the crescent with $\rho=0.8$. The incident field is polarized along x'. The numerical absorption spectra (dots) are displayed for different structure dimensions (20, 100, 200, and 300 nm). The theoretical absorption spectrum is also displayed for $D_o=20$ nm (continuous blue line).

A. Methods

All the numerical results presented have been obtained using COMSOL MULTIPHYSICS™, a commercial software implementing the finite element method. Two-dimensional simulations were performed within the harmonic propagation analysis mode in the frequency domain. Highly nonuniform adaptive meshes were used in order to model accurately the propagation of electromagnetic fields at the geometrical singularities of the nanostructures under study. The convergence of the numerical calculations with respect to the mesh size and the total simulation area has been checked. Mesh sides below 10^{-4} nm and simulation areas above 4 μm^2 were considered. As in the analytical calculations, the optical response of silver was modeled through the fit of Johnson and Christy experimental data.[37]

B. Absorption cross section

Figure 7 compares the absorption spectra normalized by D_o obtained numerically for different sizes of crescent. For a dimension of 20 nm, the quasistatic approximation is verified and a good agreement is found between the numerical and analytical results. For larger dimensions (>100 nm), radiation damping becomes important and the absorption cross section falls compared to the theoretical results: electrostatic theory predicts a scaling of σ_a as D_o^2 [Eq. (26)] which is clearly not the case here.[33] However, Fig. 7 shows that the absorption cross section remains at least on the order of the physical cross section, whatever the structure dimension, and can be even larger for $D_o=100$ nm. As already pointed out in the literature,[6] retardation effects lead to a shift of the absorption spectrum toward red compared to the electrostatic predictions (see the comparison between $D_o=20$ nm and 100 nm). Interestingly, Fig. 7 indicates that the broadband behavior of the crescent is kept and even improved for large structure dimensions.

C. Field enhancement

Figure 8 compares the field enhancement along the crescent surface ($\rho=0.8$) obtained numerically for different

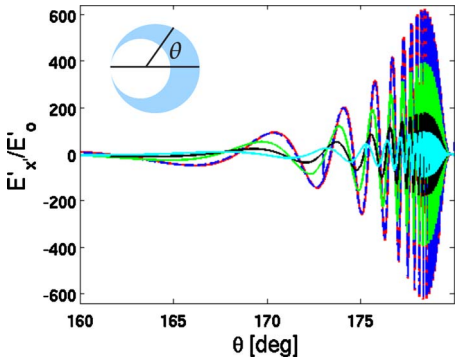

FIG. 8. (Color online) Amplitude of the x' component of the electric field at the surface of the crescent, plotted as a function of the angle, θ, defined in the figure for $\omega=0.68\omega_{sp}$ and $\rho=0.8$. The incident field is polarized along x'. The theoretical electric field [continuous red line, Eq. (28)] is compared to numerical results for different structure dimensions: 20 nm (dashed blue curve), 100 nm (green curve), 200 nm (black curve), and 300 nm (cyan curve).

structure dimensions with our theoretical prediction. The electrostatic theory states that the field enhancement does not depend on the size of the device, hence each curve can be compared on the same basis. As observed for the absorption cross section, there is a remarkable agreement between theory and the numerical result for $D_o=20$ nm. For larger structure dimension ($D_o>100$ nm), radiation damping is no longer negligible and the field enhancement falls compared to our analytical prediction. However, the device still provides a significant nanofocusing of light with a maximum enhancement factor equal to 2×10^2 for $D_o=200$ nm whereas electrostatic theory predicts 6×10^2. The nanofocusing properties of the device are thus quite robust to radiation losses. Figure 8 also shows how our theory accurately predicts the wavelength of SPPs in the crescent whatever the size of the device.

IV. CONCLUSION

To briefly conclude, this study shows how a singular conformal transformation provides an elegant tool to design a plasmonic structure capable of an efficient harvesting of light over the visible and near-infrared spectrum. Starting from an infinite slab of metal, the optical response of a cylinder with a crescent-shaped cross section has been deduced analytically. Surface-plasmon modes are shown to be excited in the fat part of the crescent and then propagate toward the tip where the group velocity vanishes and energy accumulates. This device exhibits a broadband absorption spectrum which redshifts for thinner crescents. This shift is explained by a decrease in the SPPs' velocity when the crescent gets finer. The nanofocusing performance of the device is the result of a balance between energy accumulation and dissipation losses. A strong field enhancement (up to 10^4) and confinement are predicted within the classical approach. The nanofocusing performance strongly depends on frequency (due to dissipation losses) and on the shape of the crescent (due to SPPs' velocity). Numerical simulations have shown that such plasmonic structures are robust to radiation losses. The absorption cross section is on the order of the physical cross section over the whole visible spectrum for structure dimension up to 300 nm. In addition, significant field enhancement is still induced by the structure at such dimension. The proposed plasmonic nanostructure would find great potential applications in surface-enhanced Raman scattering, single molecular detection and high-harmonic generation. The experimental challenge lies in the fabrication of such a nanostructure with a nicely shaped singularity.

ACKNOWLEDGMENTS

This work was supported by the European Community project PHOME (Contract No. 213390) and U.K. Engineering and Physical Sciences Research Council (EPSRC).

[1] G. Mie, Ann. Phys. **330**, 377 (1908).
[2] R. H. Ritchie, Phys. Rev. **106**, 874 (1957).
[3] H. Raether, *Surface Plasmons on Smooth and Rough Surfaces and on Gratings* (Springer, Berlin, 1988).
[4] U. Kreibig and M. Vollmer, *Optical Properties of Metal Clusters* (Springer, Berlin, 1995).
[5] S. A. Maier and H. A. Atwater, J. Appl. Phys. **98**, 011101 (2005).
[6] S. A. Maier, *Plasmonics: Fundamentals and Applications* (Springer, New York, 2007).
[7] J. Homola, S. S. Yee, and G. Gauglitz, Sens. Actuators B **54**, 3 (1999).
[8] W. L. Barnes, A. Dereux, and T. W. Ebbesen, Nature (London) **424**, 824 (2003).
[9] S. I. Bozhevolnyi, V. S. Volkov, E. Devaux, J.-Y. Laluet, and T. W. Ebbesen, Nature (London) **440**, 508 (2006).
[10] E. Hao and G. C. Schatz, J. Chem. Phys. **120**, 357 (2004).
[11] K. L. Kelly, E. Coronado, L. L. Zhao, and G. C. Schatz, J. Phys. Chem. B **107**, 668 (2003).
[12] F. J. García-Vidal and J. B. Pendry, Phys. Rev. Lett. **77**, 1163 (1996).
[13] J. P. Kottmann and O. J. F. Martin, Opt. Express **8**, 655 (2001).
[14] T. Atay, J.-H. Song, and V. Nurmikko, Nano Lett. **4**, 1627 (2004).
[15] P. Nordlander, C. Oubre, E. Prodan, K. Li, and M. I. Stockman, Nano Lett. **4**, 899 (2004).
[16] C. E. Talley, J. B. Jackson, C. Oubre, N. K. Grady, C. W. Hollars, S. M. Lane, T. R. Huser, P. Nordlander, and N. J. Halas, Nano Lett. **5**, 1569 (2005).
[17] L. A. Sweatlock, S. A. Maier, H. A. Atwater, J. J. Penninkhof, and A. Polman, Phys. Rev. B **71**, 235408 (2005).
[18] I. Romero, J. Aizpurua, G. W. Bryant, and F. J. García de Abajo, Opt. Express **14**, 9988 (2006).
[19] I. Romero, T. V. Teperik, and F. J. García de Abajo, Phys. Rev. B **77**, 125403 (2008).
[20] J. B. Lassiter, J. Aizpurua, L. I. Hernandez, D. W. Brandl, I.

Romero, S. Lal, J. H. Hafner, P. Nordlander, and N. J. Halas, Nano Lett. **8**, 1212 (2008).
[21] T. Härtling, Y. Alaverdyan, A. Hille, M. T. Wenzel, M. Käll, and L. M. Eng, Opt. Express **16**, 12362 (2008).
[22] L. Yang, B. Yan, and B. M. Reinhard, J. Phys. Chem. C **112**, 15989 (2008).
[23] Y. Lu, G. L. Liu, J. Kim, Y. X. Mejia, and L. P. Lee, Nano Lett. **5**, 119 (2005).
[24] J. Kim, G. L. Liu, Y. Lu, and L. P. Lee, Opt. Express **13**, 8332 (2005).
[25] H. Rochholz, N. Bocchio, and M. Kreiter, New J. Phys. **9**, 53 (2007).
[26] R. Bukasov and J. S. Shumaker-Parry, Nano Lett. **7**, 1113 (2007).
[27] B. M. Ross and L. P. Lee, Nanotechnology **19**, 275201 (2008).
[28] L. Feng, D. Van Orden, M. Abashin, Q.-J. Wang, Y.-F. Chen, V. Lomakin, and Y. Fainman, Opt. Express **17**, 4824 (2009).
[29] L. Y. Wu, B. M. Ross, and L. P. Lee, Nano Lett. **9**, 1956 (2009).
[30] G. L. Liu, Y. Lu, J. Kim, J. C. Doll, and L. P. Lee, Adv. Mater. **17**, 2683 (2005).
[31] K. Li, L. C lime, B. Cui, and T. Veres, Nanotechnology **19**, 145305 (2008).
[32] J. Zhang, Y. Fu, M. H. Chowdhury, and J. R. Lakowicz, Nano Lett. **7**, 2101 (2007).
[33] A. Aubry, D. Y. Lei, A. I. Fernández-Domínguez, Y. Sonnefraud, S. A. Maier, and J. B. Pendry, Nano Lett. **10**, 2574 (2010).
[34] G. W. Ford and W. H. Weber, Phys. Rep. **113**, 195 (1984).
[35] Y. C. Jun, R. D. Kekapture, J. S. White, and M. L. Brongersma, Phys. Rev. B **78**, 153111 (2008).
[36] B. T. Draine, Astrophys. J. **333**, 848 (1988).
[37] P. B. Johnson and R. W. Christy, Phys. Rev. B **6**, 4370 (1972).
[38] C. H. Bohren and D. R. Huffman, *Absorption and Scattering of Light by Small Particles* (Wiley, New York, 1983).
[39] Kh. V. Nerkararyan, Phys. Lett. A **237**, 103 (1997).
[40] M. I. Stockman, Phys. Rev. Lett. **93**, 137404 (2004).
[41] D. F. P. Pile, T. Ogawa, D. K. Gramotnev, T. Okamoto, M. Haraguchi, M. Fukui, and S. Matsuo, Appl. Phys. Lett. **87**, 061106 (2005).
[42] F. J. García de Abajo, J. Phys. Chem. C **112**, 17983 (2008).